Coverage Pattern Generated by Two Unicycles Pursuing Each Other

A Thesis
by

Soham Sachin Purohit
(Roll No. 190100117)

Supervisors:
Prof. Arpita Sinha
and
Prof. Anirban Guha

Department of Mechanical Engineering
Indian Institute of Technology Bombay
Mumbai 400076 (India)

24 November 2022

Declaration

I declare that this written submission represents my ideas in my own words and where others' ideas or words have been included, I have adequately cited and referenced the original sources. I declare that I have properly and accurately acknowledged all sources used in the production of this report. I also declare that I have adhered to all principles of academic honesty and integrity and have not misrepresented or fabricated or falsified any idea/data/fact/source in my submission. I understand that any violation of the above will be a cause for disciplinary action by the Institute and can also evoke penal action from the sources which have thus not been properly cited or from whom proper permission has not been taken when needed.

Soham Sachin Purohit
(Roll No. 190100117)

Date: 24 November 2022

Abstract

The objective of this thesis was to use a pair of autonomous agents modeled as unicycles to generate trajectories about a target point using control inputs that are functions of only the range between the couple. These trajectories have applications in patrolling, where the target point represents an area of interest that needs to be monitored or exploration and coverage. Through this project, we identified trajectories of interest and their purpose, and proved the conditions necessary to achieve these trajectories. Further, we also provide a methodology for achieving trajectories based on their minimum and maximum distance from the target point. Finally, we provide a variety of different trajectories generated through simulations.

Table of Contents

List of Figures

List of Tables

Chapter 1

Introduction

Taking inspiration from patterns found in nature such as fractals in clouds and animal coloration, spirals in flowers and proteins, and tesselations in crystals, researchers have used aesthetic patterns for a variety of purposes. One such class of pattern is hypotrochoids, which consist of a roulette traced by a point attached to a circle of radius r rolling around the inside of a fixed circle of radius R. In addition to their aesthetic beauty, these have found applications in a wide variety of fields, such as path planning, tool path generation, patrolling, coverage, and exploration.

In the context of using hypotrochoids for patrolling, coverage, and exploration, there exists a lot of work on single autonomous agents using linear, unicycle, and double integrator kinematic models to generate a wide variety of patterns. Different methods and control laws are employed to customize the trajectories to make them suited for different applications. In all these instances, employing multiple coordinated agents to perform this task is often considered advantageous over a single agent because it allows for a larger coverage area, a larger field of view, and a higher rate of acquiring information. This has led to several works on what is termed the 'formation control problem'.

A few methods employed in the formation control problem include the generalization of the cyclic pursuit control scheme, Hopf oscillators for multi-agent systems, consensus protocols, and the modified and improved versions of the same. All of these are intricate mathematical methods. There exists a need for a simplistic approach to the multi-agent pattern generation problem, which is the goal of this project.

Tripathy and Sinha (2018),Tripathy and Sinha (2016), and Tripathy and Sinha (2013) proposes a control scheme that only requires the range between the agent and the target point for generating patterns using a single agent having unicycle kinematics. The benefit of this control scheme is that it generates a hypotrochoid pattern for every initial condition and gain values. Further, the controller gain can be tuned to achieve a wide variety of de-

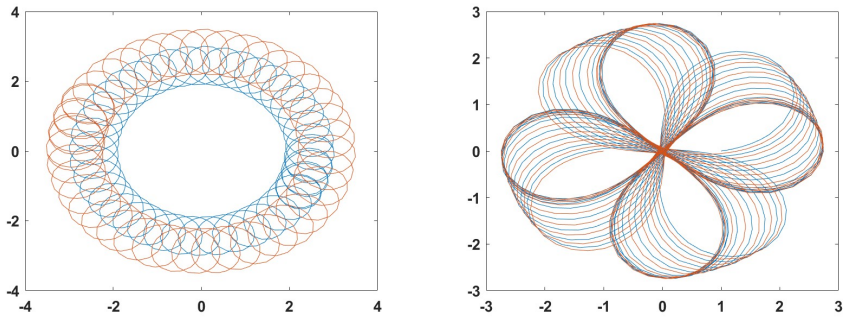

(a) (b)

Figure 1.1: Appealing trajectories generated by a pair of robots

sired trajectories to patrol the target point. Lastly, since the control scheme only requires the range information, the minimal information leads to a reduced operational cost.

This project aims to design control laws for two autonomous agents that use the range between the pair of agents instead of the range between the agents and the target point to generate trochoids with the pair of autonomous agents modeled as unicycles. The benefit of using this range instead of the previous range is that it allows the motion to remain coordinated, hence ensuring that the desired trajectories of the robots are maintained. The paper identifies desirable trajectories which maximize the benefit of using two agents instead of one and proves the conditions necessary for achieving these trajectories. It also provides a methodology for scaling the trajectories of each of the agents to customize the trajectories according to our requirements. Unlike the previous methods for generating patterns using multiple agents that are quite demanding, this provides a simplistic method for generating patterns using two agents. This also includes all the benefits of using the range-based control mentioned previously.

The contributions of the project are as follows:

- We extend the pattern formation with a single unicycle (Tripathy and Sinha, 2018) to the pattern formation with two unicycles. The extension will help us develop the theory further for multiple unicycles.

- We find the initial conditions that ensure the desired pattern formation.

The paper is organized as follows: Chapter 2 presents an extensive literature review of a few of the previous works that were the motivation for this project. Chapter 3 introduces the problem, identifies trajectories of interest, and proves conditions necessary to achieve these trajectories. Chapter 4 presents the results of a number of simulations that validates the conditions for desirable trajectories and the switching law proved in Chapter 3, and proposes future extensions of this work.

Chapter 2

Literature Survey

In this chapter, we highlight the work in a few previous papers that were the motivation behind this project. We first briefly discuss applications and other pattern-generation methods employed for the single as well as the multi-agent cases.

In Schopferer *et al.* (2018), trochoids have been used for path planning of fixed-wing unmanned aircraft in uncertain wind conditions. Zhou *et al.* (2016) and Xu *et al.* (2019) use trochoids for tool path generation for inspecting surfaces and material removal on a surface. Trochoids also find wide use in patrolling, coverage, and exploration. In Coombes *et al.* (2018), the problem of coverage of a fixed-wing UAV has been tackled by using an optimal polygon decomposition method. Employing multiple coordinated agents to perform this task is often considered advantageous over a single agent because it allows for a larger coverage area, a larger field of view, and a higher rate of acquiring information. There exists a lot of work on single agents using linear, unicycle, and double integrator kinematic models to generate a wide variety of patterns. In Monsingh and Sinha (2019), trochoidal patterns are generated by multiple agents with single-integrator kinematics using a generalized consensus strategy based on Tsiotras and Castro (2014) and Tsiotras and Reyes Castro (2013). In Parayil and Ratnoo (2019), trochoids are generated using an agent with unicycle dynamics having a control law with parameters that cause the dynamics to exhibit supercritical Andronov-Hopf bifurcation.

There also exists a lot of work on the formation control problem. Through Ansart and Juang (2020b), Ansart and Juang (2020a), and Juang (2013), Juang uses single-integrator kinematics to propose a generalization of the cyclic pursuit control scheme and its extension thereafter. In Ansart and Juang (2021), the generalized cyclic pursuit law is used to maintain a group of agents in an epicycle-like formation. Ramachandran and Juang (2021) uses a Hopf oscillator for the multi-agent system to improve the robustness as compared to the cyclic pursuit control scheme. Tsiotras and Reyes Castro (2011) uses an

extension of the standard consensus protocol for generating periodic and quasi-periodic patterns. Tripathy and Sinha (2018), Tripathy and Sinha (2016), and Tripathy and Sinha (2013) propose a control scheme that only requires the range between the agent and the target point for generating patterns using a single agent having unicycle kinematics. These works have been highlighted further ahead since these are the primary motivations behind the project. The benefit of this control scheme is that it generates a hypotrochoid pattern for every initial condition and gain values. Further, the controller gain can be tuned to achieve a wide variety of desired trajectories to patrol the target point. Lastly, since the control scheme only requires the range information, the minimal information leads to a reduced operational cost.

An application using range-only measurements is Boyinine *et al.* (2019), in which range-only measurements are used for the landing control of a UAV on a moving ship.

We now discuss the primary motivation in greater detail.

2.1 Guidance of an Autonomous Agent for Coverage Applications using Range Only Measurement

The paper Tripathy and Sinha (2013) was the first paper that addressed the problem of single-agent pattern generation using a range-only control scheme. It uses the simple control scheme of:

$$u(t) = kr(t) \tag{2.1}$$

$R_{\min}$ and $R_{\max}$ were determined for this control law given any initial conditions. Further, if $R_{\min}$ and $R_{\max}$ are given, the conditions necessary to cover this region of interest were determined. It was observed that for some values of the initial parameters, a circular trajectory was achieved by the unicycle whose radius depended upon the initial conditions. Finally, the effect of varying the initial parameters was studied and presented. Some simulations were displayed to validate the previous results.

2.2 Generating Patterns With a Unicycle

The reference Tripathy and Sinha (2016) addresses the problem of making a unicycle trace hypotrochoid-like patterns using a simple range-based control scheme. The scheme used in this paper is:

$$u(t) = \eta r^{\mu}(t) \tag{2.2}$$

It proves that with the given control scheme and any gain, the unicycle achieves a hypotrochoid pattern always. The patterns are characterized based on the minimum and

maximum distances achieved by the unicycle from the target point. Conditions are determined for when the unicycle achieves the minimum and maximum distance from the target point. Further, the paper also determines the controller gains necessary to achieve any hypotrochoid pattern as desired using a switching law, that is, a law that changes the controller gain from an initial to a final value at a predefined value of r to ensure that the pattern traced lies within a certain set of values. The paper also determines whether a pattern can be achieved by the unicycle based on turn-rate constraints imposed on the unicycle. Finally, the work is validated by presenting simulation results.

2.3 Unicycle With Only Range Input: An Array of Patterns

The reference Tripathy and Sinha (2018) is an extension and generalization of Tripathy and Sinha (2016). The objective is again to generate planar hypotrochoid patterns by a unicyclic autonomous agent using the general range-based control scheme-

$$u(t) = f(t) \tag{2.3}$$

The paper characterizes the trajectories into five types based on the control law, initial conditions, and the velocity of the unicycle. These five types determine the type of trajectory, whether a hypotrochoid is generated, or an unbounded spiral. For the cases where a hypotrochoid is produced, the paper provides a methodology to determine the minimum and maximum distance from the target point achieved by the unicycle. A methodology for designing control for producing annular trajectories is proposed. This includes designing the control law and a switching strategy, the combination of which, produces an annular trajectory confined within the desired minimum and maximum distance from the target point. Finally, the results are validated through simulations and some appealing trajectories are displayed along with their generating control functions.

Chapter 3

Analysis and Methods

3.1 Problem Description

In this project, we consider the patterns generated by a pair of robots patrolling a target point $\mathcal{T}$. We use a control law that requires only the range (given by r) , which is the line-of-sight (LOS) distance of one robot from the other. This planar geometry is depicted in Fig. 3.1, in which $\mathcal{R}_1$ and $\mathcal{R}_2$ denote the first and second robots respectively, v_1 and v_2 denote their corresponding velocity vectors, α_1 and α_2 are their corresponding heading directions, r is the distance between $\mathcal{R}_1$ and $\mathcal{R}_2$, and $\mathcal{T}$ is the target point (assumed to be at the origin without loss of generality).
We assume that both the robots are modeled as unicycles and hence have the kinematics governed by the following equations-

$$\dot{x}_i(t) = v_i cos(\alpha_i),\ \dot{y}_i(t) = v_i sin(\alpha_i),\ \dot{\alpha}_i(t) = u_i(t) \tag{3.1}$$

where $i = 1, 2$, (x_i,y_i) are the locations of $\mathcal{R}_i$ with respect to the global frame respectively, and u_i is the input. We consider that the input only requires the range, and hence, we consider the control designed as

$$u_i(t) = \eta r^{\mu}(t), \quad i = 1, 2 \tag{3.2}$$

where $\eta \neq 0$ is the controller gain and μ is a positive constant.

3.2 Analysis of Trajectories

We are interested in trajectories that will enable robots to have as much field of view as possible at any time during the patrolling. To ensure that the combined field of view of the robots is large, the robots must be located on either side of the target point.

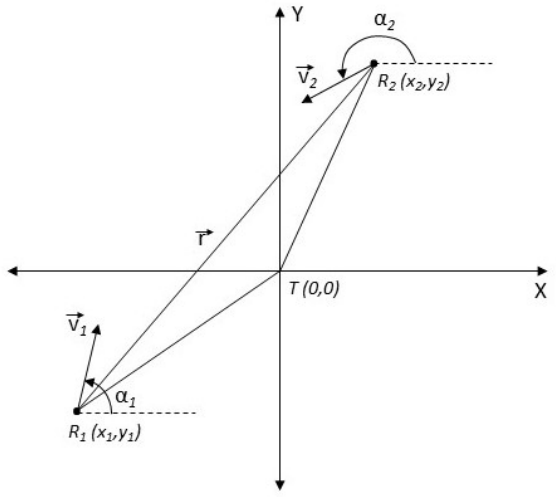

Figure 3.1: General setup of the problem with the two robots $\mathcal{R}_1$ and $\mathcal{R}_2$ rotating about the stationary point $\mathcal{T}$ with only range r as input

3.2.1 Trajectories of Interest

Proposition 1 *For the two robots with kinematics* (3.1) *following the control law* (3.2)*, the target point $\mathcal{T}$ remains at the mid-point of the two robots for all time if $v_1 = v_2$ and the initial conditions satisfy*

$$v_1 = v_2 \tag{3.3}$$

$$[x_{10}, y_{10}]^T = -[x_{20}, y_{20}]^T \tag{3.4}$$

$$\alpha_{10} = \alpha_{20} \pm \pi \tag{3.5}$$

where (x_{i0}, y_{i0}) and α_{i0} are the position and heading of robot i at the time $t = 0$.

Proof: To prove that the target point, $\mathcal{T}$= (0,0) remains at the midpoint of the two robots for all times, we need to show that at $t = 0$, the midpoint is at $\mathcal{T}$ and the rate of change of the position of the midpoint is zero at all times. Equation (3.4) establishes that the midpoint at $t = 0$ is at (0,0). To show that the midpoint remains constant for all time, let $x_m = (x_1 + x_2)/2$, $y_m = (y_1 + y_2)/2$ and $v_1 = v_2 = v$. From (3.1) and (3.2), $\dot{\alpha}_1 = \dot{\alpha}_2$. Hence, we can write

$$\alpha_i(t) = F(t) + \alpha_{i,0}, \quad i = 1, 2 \tag{3.6}$$

where $F(t) = \int_0^t \eta r^{\mu}(\tau) d\tau$. Now, from (3.1),

$$\begin{aligned}\dot{x}_m =& v\left(\frac{\cos\alpha_1 + \cos\alpha_2}{2}\right) = \{\cos F(t)(\cos\alpha_{10} + \cos\alpha_{20}) \\ & - \sin F(t)(\sin\alpha_{10} + \sin\alpha_{20})\}\frac{v}{2} \qquad (3.7)\\ \dot{y}_m =& v\left(\frac{\sin\alpha_1 + \sin\alpha_2}{2}\right) = \{\sin F(t)(\cos\alpha_{10} \\ & + \cos\alpha_{20}) + \cos F(t)(\sin\alpha_{10} + \sin\alpha_{20})\}\frac{v}{2} \qquad (3.8)\end{aligned}$$

Applying (3.5), we get $\dot{x}_m = 0$ and $\dot{y}_m = 0$, implying that the midpoint remains at $\mathcal{T}$ for all time. ■

When $v_1 \neq v_2$, the midpoint of the robots will not remain stationary. But we show next that another point (x_f, y_f) remains fixed in space, which is given by the linear combination of the instantaneous positions of the robots.

$$x_f = \left(\frac{v_2}{v_1 + v_2}\right)x_1 + \left(\frac{v_1}{v_1 + v_2}\right)x_2 \qquad (3.9)$$

$$y_f = \left(\frac{v_2}{v_1 + v_2}\right)y_1 + \left(\frac{v_1}{v_1 + v_2}\right)y_2 \qquad (3.10)$$

We define the initial conditions such that the fixed point (x_f, y_f) remains at $\mathcal{T}$ for all time in the following corollary.

Corollary 1 *When $v_1 \neq v_2$, (x_f, y_f) remains at $\mathcal{T}$ for all time if the initial positions satisfy*

$$v_2[x_{10}, y_{10}]^T + v_1[x_{10}, y_{20}]^T = 0 \qquad (3.11)$$

and (3.5) *is satisfied.*

Proof: At $t = 0$, (x_f, y_f) coincides with $\mathcal{T}$ by the conditions of the Corollary. Taking derivatives

$$\dot{x}_f = \frac{v_1 v_2}{v_1 + v_2}(\cos\alpha_1 + \cos\alpha_2) \qquad (3.12)$$

$$\dot{y}_f = \frac{v_1 v_2}{v_1 + v_2}(\sin\alpha_1 + \sin\alpha_2) \qquad (3.13)$$

Applying (3.5) and (3.6), we can see that $\dot{x}_f = 0$ and $\dot{y}_f = 0$. Therefore, (x_f, y_f) remains fixed in space for all time and the fixed point is $\mathcal{T}$ by the selection of initial conditions. ■

Remark 1 *For any initial conditions that do not satisfy* (3.11)*, the robots will not encircle $\mathcal{T}$. Instead, they will encircle a point (x_f, y_f) given in* (3.9) *and* (3.10)*.*

Remark 2 *Proposition 1 and Corollary 1 hold for any $u_i(t), i = 1, 2$ as long as it is a function of the LOS distance r only.*

Next, we study the trajectories of the robots with respect to the target point $\mathcal{T}$. The point $\mathcal{T}$ lies on the line joining the instantaneous positions of the robots. Let us denote the distance between the robot $\mathcal{R}_i$ and $\mathcal{T}$ by r_i for $i = 1, 2$. We can find a control law as a function of r_i equivalent to (3.2).

Proposition 2 *Let the robots follow the target $\mathcal{T}$ with control*

$$u_i = \overline{\eta}_i r_i^{\mu}, \quad i = 1, 2 \tag{3.14}$$

with $\overline{\eta}_i = \eta \left(\frac{v_1+v_2}{v_i}\right)^{\mu}$.Then, the trajectories of robots will be the same as their trajectories under the control law (3.2) *for the same initial conditions.*

Proof: It is easy to see from (3.9) and (3.10) that

$$r_i = \sqrt{(x_f - x_i)^2 + (y_f - y_i)^2} = \frac{v_i}{v_1 + v_2} r \tag{3.15}$$

Hence, (3.14) is $u_i = \eta r^{\mu}$. This implies that the robots are governed by the same control law as in (3.2). Given the same initial conditions, they will follow the same trajectory as the robots under control (3.2). ■

The control law (3.14) for robot $\mathcal{R}_i$ is the same as the control law developed for a single robot in Tripathy and Sinha (2016). The robot in Tripathy and Sinha (2016) traces a hypotrochoidal pattern about $\mathcal{T}$ with a specified maximum and minimum radius. We can similarly find the patterns formed by the pair of robots.

3.2.2 Minimum and Maximum Distance From Center

Now that we have determined conditions to ensure that the robots are at the maximum possible distance from each other, we now determine the maximum (R_{max}) and minimum (R_{min}) distances of the robot from the stationary point, based on the initial conditions. From Tripathy and Sinha (2018), we get the method to determine the R_{max} and R_{min} for a single robot rotating about a stationary point with only range as input. This can be easily extended to the two robot case when the velocities of the two robots are equal. Note that because the motion is symmetric as proved in Proposition 1, the distance of either robot from the stationary point is always half of the distance from the other robot. This implies that at any time during the motion, the input acting on the robot is always twice of what it would have been in the single robot case. Hence, we can get R_{max} and R_{min} by simply using $2u(t)$ in place of $u(t)$ and using the method described in Tripathy and Sinha (2018).

As an example, we take the case of $\mu = 1$ and $\eta = 1$ in (3.2) to determine R_{max} and R_{min}, which we will verify in Chapter 4. As previously mentioned, the control law would

be twice that in the two robot case, hence, $u(t) = 2r(t)$. R_{max} and R_{min} are given by the intersection of $g_k(r)$ with the lines vr and $-vr$. Where-

$$g_k(r) = \tilde{f}(r) - K \tag{3.16}$$

$$\tilde{f}(r) = \int 2ru(t)dr \tag{3.17}$$

$$K = \tilde{f}(r_0) + vr_0 sin\phi_0 \tag{3.18}$$

Here, r_0 is the initial condition for the distance between the two robots and $\phi_0 = \alpha_0 - \theta_0$, where θ is the line-of-sight angle of $\mathcal{T}$ from the robot.
In our case, (3.17) becomes:

$$\tilde{f}(r) = \frac{2}{3}r^3 \tag{3.19}$$

Hence, R_{max} and R_{min} are given by solving for positive r the following equations. Note that these equations will only have two positive roots in total always since the cubic function is monotonically increasing. The smaller of these roots is R_{min} while the larger is R_{max}.

$$\frac{2}{3}r^3 - K = vr \tag{3.20}$$

$$\frac{2}{3}r^3 - K = -vr \tag{3.21}$$

We now extend the previous result to situations when the two robots have unequal speeds. Note that because the motion is symmetric as proved in Corollary 1, the distance of the first robot from the stationary point is always $\frac{v_1}{v_1+v_2}$ of the distance from the second robot and the distance of the second robot from the stationary point is always $\frac{v_2}{v_1+v_2}$ of the distance from the first robot. This implies that at any time during the motion, the input acting on the first robot is always $\frac{v_1+v_2}{v_1}$ of what it would have been in the single robot case while it is $\frac{v_1+v_2}{v_2}$ times for the second robot. Hence, we can get R_{max} and R_{min} by simply using $\frac{v_1+v_2}{v_1}u(t)$ in place of $u(t)$ for the first robot and $\frac{v_1+v_2}{v_2}u(t)$ in place of $u(t)$ for the second robot using the method described in Tripathy and Sinha (2018). Hence, when we consider the case of $v_1 = 1$ and $v_2 = 2$ in the example considered above, (18), (20), (21), (22) for the second robot become-

$$\tilde{f}(r) = \int \frac{3}{2}ru(t)dr \tag{3.22}$$

$$\tilde{f}(r) = \frac{1}{2}r^3 \tag{3.23}$$

$$\frac{1}{2}r^3 - K = vr \tag{3.24}$$

$$\frac{1}{2}r^3 - K = -vr \tag{3.25}$$

Solving for r in (3.24) and (3.25) gives us the R_{max} and R_{min} for this case

3.2.3 Switching Law to Constrain the Motion of the Robots

The previous section allowed us to only determine the maximum and the minimum distances of the robots in the trajectory based on the initial condition. However, it did not give us a methodology for obtaining desired trajectories based on a desired R_{max} and R_{min}. In this section, we obtain this methodology.

Let the maximum and minimum radius of the annulus formed by robot $\mathcal{R}_i$ be $R_{i\max}$ and $R_{i\min}$, respectively. Using (3.15), we have

$$\frac{R_{1\max}}{R_{2\max}} = \frac{R_{1\min}}{R_{2\min}} = \frac{v_1}{v_2} \tag{3.26}$$

Therefore, given v_1 and v_2, we can have user-defined values for any two of the four radii, $R_{1\max}$, $R_{2\max}$, $R_{1\min}$ and $R_{2\min}$. The other two get fixed by (3.26).

Theorem 1 *Consider a pair of robots satisfying the initial condition* (3.11)*. Each robot $\mathcal{R}_i$ will trace a hypotrochoidal pattern with maximum and minimum radii $R_{i\max}$ and $R_{i\min}$, respectively, if the controller gain is switched from η_i to η_i', where η_i and η_i' take one of the four possible values*

$$\eta_{i1} = \frac{(\mu+2)v_i^{\mu+1}}{(v_1+v_2)^{\mu}}\left\{\frac{R_{i\max}^{\mu+2}(r_{10}sin\phi_{10} - R_{i\min})}{(r^{\mu+2}-r_{10}^{\mu+2})(R_{i\max}^{\mu+2}-R_{i\min}^{\mu+2})} + \frac{-R_{i\min}^{\mu+2}(r_{10}sin\phi_{10}+R_{i\max}) + r^{\mu+2}(R_{i\max}+R_{i\min})}{(r^{\mu+2}-r_{10}^{\mu+2})(R_{i\max}^{\mu+2}-R_{i\min}^{\mu+2})}\right\}$$

$$\eta_{i1}' = \left(\frac{(\mu+2)v_i^{\mu+1}}{(v_1+v_2)^{\mu}}\right)\left(\frac{R_{i\max}+R_{i\min}}{R_{i\max}^{\mu+2}-R_{i\min}^{\mu+2}}\right) \tag{3.27}$$

$$\eta_{i2} = \frac{(\mu+2)v_i^{\mu+1}}{(v_1+v_2)^{\mu}}\left\{\frac{R_{i\max}^{\mu+2}(r_{10}sin\phi_{10} + R_{i\min})}{(r^{\mu+2}-r_{10}^{\mu+2})(R_{i\max}^{\mu+2}-R_{i\min}^{\mu+2})} + \frac{-R_{i\min}^{\mu+2}(r_{10}sin\phi_{10}+R_{i\max}) + r^{\mu+2}(R_{i\max}-R_{i\min})}{(r^{\mu+2}-r_{10}^{\mu+2})(R_{i\max}^{\mu+2}-R_{i\min}^{\mu+2})}\right\}$$

$$\eta_{i2}' = \left(\frac{(\mu+2)v_i^{\mu+1}}{(v_1+v_2)^{\mu}}\right)\left(\frac{R_{i\max}-R_{i\min}}{R_{i\max}^{\mu+2}-R_{i\min}^{\mu+2}}\right) \tag{3.28}$$

$$\eta_{i3} = \frac{(\mu+2)v_i^{\mu+1}}{(v_1+v_2)^{\mu}}\left\{\frac{R_{i\max}^{\mu+2}(r_{10}sin\phi_{10} + R_{i\min})}{(r^{\mu+2}-r_{10}^{\mu+2})(R_{i\max}^{\mu+2}-R_{i\min}^{\mu+2})} - \frac{R_{i\min}^{\mu+2}(r_{10}sin\phi_{10}-R_{i\max}) + r^{\mu+2}(R_{i\max}+R_{i\min})}{(r^{\mu+2}-r_{10}^{\mu+2})(R_{i\max}^{\mu+2}-R_{i\min}^{\mu+2})}\right\}$$

$$\eta_{i3}' = -\left(\frac{(\mu+2)v_i^{\mu+1}}{(v_1+v_2)^{\mu}}\right)\left(\frac{R_{i\max}+R_{i\min}}{R_{i\max}^{\mu+2}-R_{i\min}^{\mu+2}}\right) \tag{3.29}$$

$$\eta_{i4} = \frac{(\mu+2)v_i^{\mu+1}}{(v_1+v_2)^{\mu}}\left\{\frac{R_{i\max}^{\mu+2}(r_{10}sin\phi_{10} - R_{i\min})}{(r^{\mu+2} - r_{10}^{\mu+2})(R_{i\max}^{\mu+2} - R_{i\min}^{\mu+2})}\right.$$
$$\left. - \frac{R_{i\min}^{\mu+2}(r_{10}sin\phi_{10} - R_{i\max}) + r^{\mu+2}(R_{i\max} - R_{i\min})}{(r^{\mu+2} - r_{10}^{\mu+2})(R_{i\max}^{\mu+2} - R_{i\min}^{\mu+2})}\right\}$$
$$\eta'_{i4} = -\left(\frac{(\mu+2)v_i^{\mu+1}}{(v_1+v_2)^{\mu}}\right)\left(\frac{R_{i\max} - R_{i\min}}{R_{i\max}^{\mu+2} - R_{i\min}^{\mu+2}}\right) \tag{3.30}$$

v_i is the velocity of R_i, r_{i0} is the initial value of r_i, $\phi_{i0} = \alpha_{i0} - arctan2\,(-y_{i0}, -x_{i0})$ and $R_{1\max}$, $R_{1\min}$, $R_{2\max}$, $R_{2\min}$ satisfy (3.26).

Proof: Theorem 1 of Tripathy and Sinha (2016) gives us a switching law for enabling the trajectory to remain within a given $[R_{\min}, R_{\max}]$ for the case of a single unicycle using a range input. In Proposition 2, we showed that the motion of each of the robots in the two-robot case is equivalent to a single-robot case. Hence, the switching law in Tripathy and Sinha (2016) applies to $\overline{\eta}$, which is the corresponding gain for the single robot case. However, we need the switching law for η. 3.14 gives us the relation between η and $\overline{\eta}$. Hence, if $\overline{\eta}$ goes from some value $\overline{\eta_i}$ to $\overline{\eta_i}'$, η will go from $(v_i/(v_1+v_2))^{\mu}$ $\overline{\eta_i}$ to $(v_i/(v_1+v_2))^{\mu}$ $\overline{\eta_i}'$. Hence, by multiplying the factor of $(v_i/v_1+v_2)^{\mu}$ to the switching strategy, we get the corresponding switching strategy for both the robots in the two robot case. ■

In this chapter, we have identified trajectories of interest and proved the conditions necessary to achieve the same. Next, we have determined the minimum and maximum distance from the center of the annulus achieved by the robots based on the initial conditions. Finally, we have proposed and proved a switching scheme to ensure that the two robots remain confined to a certain distance from the center of the annulus to customize trajectories as desired. In the next chapter, we validate the results proved above.

Chapter 4

Results and Discussions

4.1 Simulation Results

Simulations were run to verify the conditions for favorable trajectories proved above, to check R_{max} and R_{min} calculations in the robot trajectories, and for verifying the switching law. For each verification, a number of different initial parameters that satisfied the conditions were tried. For each of the simulations, the control law (3.2) is considered with $\eta = 1$ and $\mu = 1$. The blue lines indicate the trajectory followed by $\mathcal{R}_1$ and the violet lines indicate the trajectory followed by $\mathcal{R}_2$. The black and the red dots indicate the starting positions of $\mathcal{R}_1$ and $\mathcal{R}_2$ respectively, while the yellow and the green dots indicate the ending positions.

4.1.1 Equal speeds, symmetric trajectory

To verify Propositon 2, the speeds of the two robots were kept constant with $\eta = 1$ and $\mu = 1$ and the other initial conditions were varied with (3.4) and (3.5) always satisfied. Table 4.1 lists the initial conditions for all the simulated cases.

The results of the simulations are displayed in Fig. 4.2. Here, we observe that the trajectory is such that $\mathcal{T}(0,0)$ divides both the points on the trajectories of the two robots

	v	(x_{10}, y_{10})	(x_{20}, y_{20})	α_{10}	α_{20}
Case a	5	(1,0)	(-1,0)	30°	210°
Case b	5	(1,-2)	(-1,2)	45°	225°
Case c	5	(3,-2)	(-2,3)	60°	240°
Case d	5	(4,-4)	(-4,4)	90°	270°

Table 4.1: Equal Speed Cases

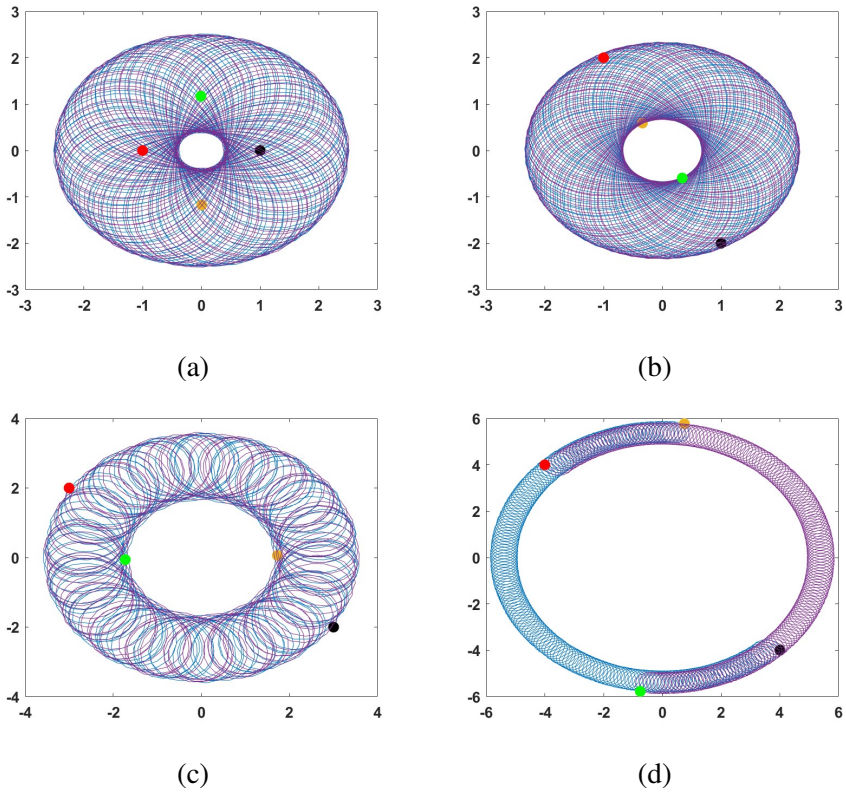

(a) (b)

(c) (d)

Figure 4.1: Equal speeds, symmetric trajectory

The results of the simulations are displayed in Fig. 4.1. We observe that in each of the cases, the starting and the ending points have the stationary point $\mathcal{T}$ as their midpoint. Both the robots follow an annular trajectory with the center as $\mathcal{T}$. This verifies Proposition 2.

4.1.2 Unequal speeds, symmetric trajectory

In this section, the speeds of the two robots are unequal with the conditions of Corollary 1 satisfied for each of the following cases as displayed in Table 4.2

	v_1	v_2	(x_{10}, y_{10})	(x_{20}, y_{20})	α_{10}	α_{20}
Case a	1	2	(-1,1)	(2,-2)	30°	210°
Case b	6	2	(3,0)	(-1,0)	90°	270°
Case c	3	4	(3,0)	(-4,0)	90°	270°
Case d	3	4	(0.45,0.3)	(-0.6,-0.4)	45°	225°

Table 4.2: Unequal Speed Cases

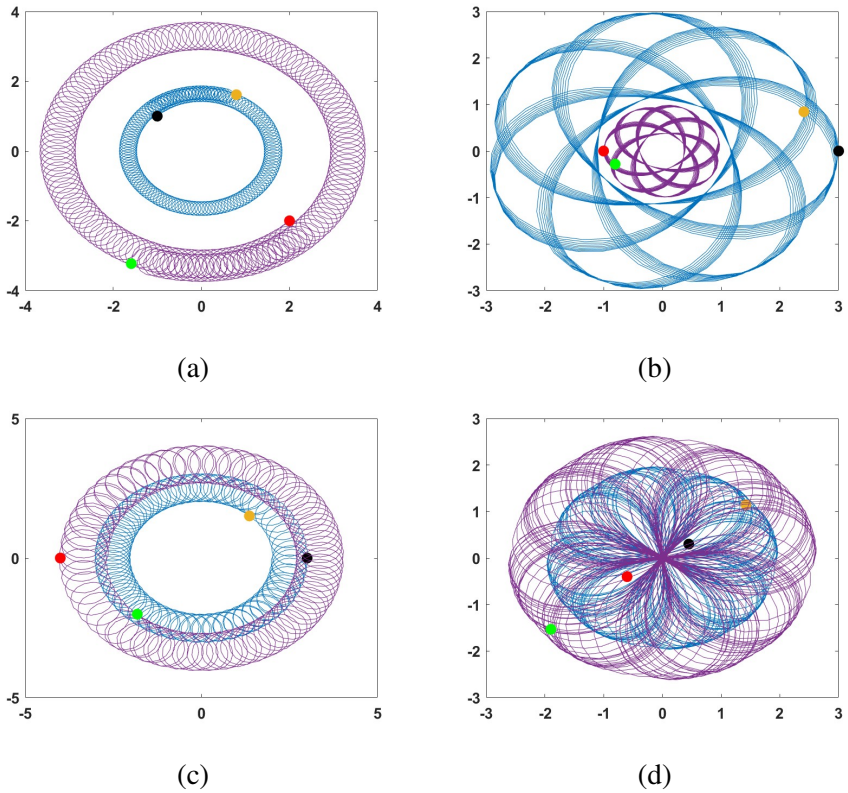

(a) (b)

(c) (d)

Figure 4.2: Unequal speeds, symmetric trajectory

in the ratio $v_1 : v_2$. Both the robots follow an annular trajectory with the center as $\mathcal{T}$. This verifies Corollary 1.

4.1.3 Determining R_{max} and R_{min} for the equal speeds, symmetric trajectory cases

We now calculate R_{max} and R_{min} for the four cases from subsection 4.1.1 and verify the results with the graphs from Fig. 4.1. We calculate r_0, ϕ_0, K, R_{min}, and R_{max} by using the method described in Chapter 3. K is found by using (3.17) and (3.18). After calculating K, the positive roots of (3.20) and (3.21) give R_{min} and R_{max}. The results are tabulated in 4.3.

Comparing these results to the graphs obtained in Fig. 4.1, we see that the results match. This validates the extension of the single robot trajectories to the two robot case.

4.1.4 Determining R_{max} and R_{min} for the unequal speeds, symmetric trajectory cases

We now calculate R_{max} and R_{min} for both robots in the four cases from subsection 4.1.2 and verify the results with the graphs from Fig. 4.2. The appropriate factor is

	r_0	ϕ_0	K	$R_{\min}$	$R_{\max}$
Case a	1	$-150°$	-1.83	0.37	2.53
Case b	2.24	$-71.57°$	-3.15	0.67	2.34
Case c	3.61	$-98.86°$	13.44	1.85	3.62
Case d	5.66	$-45°$	100.68	4.86	5.79

Table 4.3: $R_{\min}$ and $R_{\max}$ for equal speed cases

	r_{10}	ϕ_{10}	K_1	$R_{1\,\min}$	$R_{1\,\max}$	r_{20}	ϕ_{20}	K_2	$R_{2\,\min}$	$R_{2\,\max}$
Case a	1.41	$-285°$	4.19	1.41	1.82	2.83	$75°$	16.78	2.84	3.64
Case b	3	$-90°$	-6	1.1	3	1	$270°$	-0.67	0.37	1
Case c	3	$-90°$	12	1.98	3	4	$270°$	21.33	2.64	4
Case d	0.54	$-168.69°$	-0.20	0.07	1.93	0.72	$191.31°$	-0.35	0.09	2.57

Table 4.4: $R_{\min}$ and $R_{\max}$ for unequal speed cases

substituted in place of 2 in (3.17) as mentioned in Chapter 3. The method remains the same from this point.

Comparing these results to the graphs obtained in Fig. 4.2, we see that the results match. This validates the analysis done for the case of robots with unequal speeds.

4.1.5 Verification of Switching Law

Here we consider two cases, one where the speeds are the same and the other where the speeds are different. When the speeds are the same, both robots trace the same annulus. We specify the desired annulus by $R_{\max} = 10$ and $R_{\min} = 6$. The initial condition is given in Table 4.5 case 1. Using Theorem 1, we calculate the controller gain for switching at $r = 5$ and get $\eta = 0.1531$ to $\eta' = 0.0782$. Figure 4.3 (a) shows the trajectories of the robots and Figure 4.3 (b) shows the evolution of the trajectories with time. The change in trajectory can be clearly seen along with the desired $R_{\max}$ and $R_{\min}$ being achieved
In the second case, we keep the speeds of the robots different and specify the desired annulus for $\mathcal{R}_1$ by $R_{1\,\max} = 8$ and $R_{1\,\min} = 4$. The initial condition is given in Table 4.5 case 2. We calculate the controller gain as before for switching at $r = 4$ and get $\eta_{11} = 0.0068$ to $\eta'_{11} = 0.0643$. Figure 4.4 shows the trajectories of the robots and the evolution of the trajectories with time in (a) and (b) respectively. We observe the change in trajectory when the switch takes place along with the desired $R_{\max}$ and $R_{\min}$ for $\mathcal{R}_1$, represented by the blue line, being achieved. Further, we can also see that the motion of $\mathcal{R}_2$ is proportionally scaled to the speeds, and the $R_{2\,\max}$ and $R_{2\,\min}$ according to (3.26) is achieved.

	v_1	v_2	(x_{10}, y_{10})	α_{10}	$R_{\max}$	$R_{\min}$	r
Case 1	5	5	(9,0)	10°	10	6	5
Case 2	2	3	(8,0)	20°	8	4	4

Table 4.5: Switching law cases

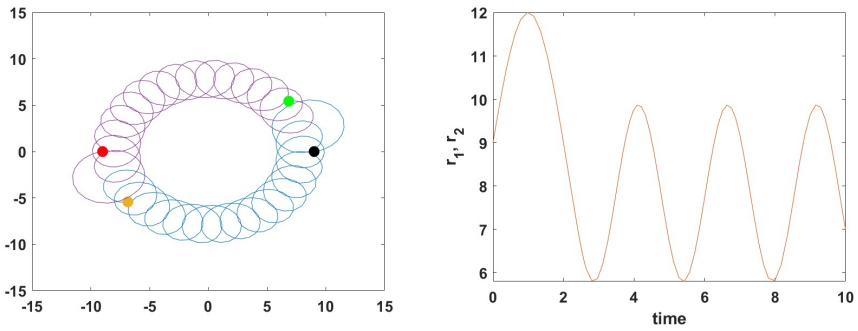

(a) (b)

Figure 4.3: Evolution of Trajectory for Case 1 of the switching law

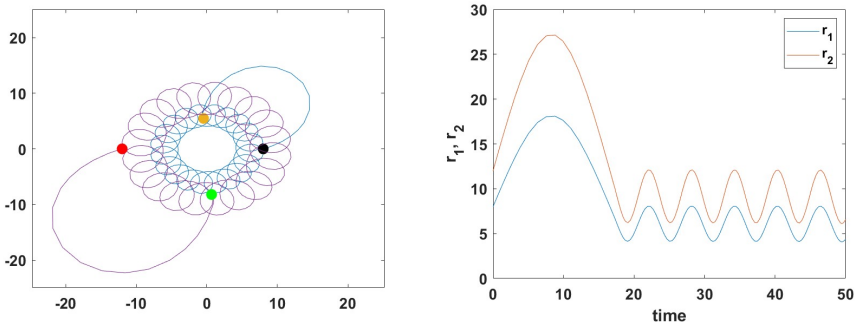

(a) (b)

Figure 4.4: Evolution of Trajectory for Case 2 of the switching law

4.2 Conclusion

Through this project, we were able to extend a simple range-based control scheme for generating hypotrochoids from a single agent to a double agent case. Not only does this provide a simplistic methodology for generating patterns using multiple agents, but also includes the advantages of using a range-only based control scheme, such as producing hypotrochoids for all values of the initial conditions and a reduced operational cost. In this, we first identified trajectories that maximize the coverage area and subsequently prove the conditions needed to achieve the same. Next, we determined R_{max} and R_{min} from the initial conditions. Finally, we proposed a switching scheme for ensuring that the patrolling of the pair of robots remains within the desired range of values. We also validated all of the propositions mentioned above through simulations. This work on the two-agent case paves the way for generalizing to the multi-agent pattern generation case in which the number of agents is as desired.

References

Ansart, A., and Juang, J.-C., 2020a, "Generalized cyclic pursuit: A model-reference adaptive control approach," in *2020 5th International Conference on Control and Robotics Engineering (ICCRE)*, pp. 89–94.

Ansart, A., and Juang, J.-C., 2020b, "Generalized cyclic pursuit: An estimator-based model-reference adaptive control approach," in *2020 28th Mediterranean Conference on Control and Automation (MED)*, pp. 598–604.

Ansart, A., and Juang, J.-C., 2021, "Integral sliding control approach for generalized cyclic pursuit formation maintenance," *Electronics* **10**, doi:\bibinfo{doi}{10.3390/electronics10101217}

Boyinine, R., Chakraborty, A., Sharma, R., and Brink, K., 2019, "Development of sliding-mode landing controller using cooperative relative localization with pattern generation," in *2019 Sixth Indian Control Conference (ICC)*, pp. 128–133.

Coombes, M., Fletcher, T., Chen, W.-H., and Liu, C., 2018, "Optimal polygon decomposition for uav survey coverage path planning in wind," *Sensors* **18**

Juang, J.-C., 2013, "On the formation patterns under generalized cyclic pursuit," *IEEE Transactions on Automatic Control* **58**, 2401–2405.

Monsingh, J. M., and Sinha, A., 2019, "Trochoidal patterns generation using generalized consensus strategy for single-integrator kinematic agents," *European Journal of Control* **47**, 84–92.

Parayil, A., and Ratnoo, A., 2019, "Bifurcation-based control law for pattern generation," *IEEE Control Systems Letters* **3**, 374–379.

Ramachandran, K., and Juang, J.-C., 2021, "Application of oscillator dynamics for deviated pursuit formations: Preliminary results," in *2021 International Automatic Control Conference (CACS)*, pp. 1–6.

Schopferer, S., Lorenz, J. S., Keipour, A., and Scherer, S., 2018, "Path planning for unmanned fixed-wing aircraft in uncertain wind conditions using trochoids," in *2018 International Conference on Unmanned Aircraft Systems (ICUAS)*, pp. 503–512.

Tripathy, T., and Sinha, A., 2013, "Guidance of an autonomous agent for coverage applications using range only measurement," in *AIAA Guidance, Navigation, and Control (GNC) Conference*

Tripathy, T., and Sinha, A., 2016, "Generating patterns with a unicycle," *IEEE Transactions on Automatic Control* **61**, 3140–3145.

Tripathy, T., and Sinha, A., 2018, "Unicycle with only range input: An array of patterns," *IEEE Transactions on Automatic Control* **63**, 1300–1312.

Tsiotras, P., and Castro, L., 2014 01, "The artistic geometry of consensus protocols," ISBN 978-3-319-03903-9, pp. 129–153.

Tsiotras, P., and Reyes Castro, L. I., 2011, "Extended multi-agent consensus protocols for the generation of geometric patterns in the plane," in *Proceedings of the 2011 American Control Conference*, pp. 3850–3855.

Tsiotras, P., and Reyes Castro, L. I., 2013, "A note on the consensus protocol with some applications to agent orbit pattern generation," in *Distributed Autonomous Robotic Systems: The 10th International Symposium*, edited by Martinoli, A., Mondada, F., Correll, N., Mermoud, G., Egerstedt, M., Hsieh, M. A., Parker, L. E., and Støy, K. (Springer Berlin Heidelberg, Berlin, Heidelberg). ISBN 978-3-642-32723-0, pp. 345–358.

Xu, C.-Y., Li, J.-R., Liang, Y.-J., Wang, Q.-H., and Zhou, X.-F., 2019, "Trochoidal toolpath for the pad-polishing of freeform surfaces with global control of material removal distribution," *Journal of Manufacturing Systems* **51**, 1–16.

Zhou, Z., Zhang, Y., and Tang, K., 2016, "Sweep scan path planning for efficient freeform surface inspection on five-axis cmm," *Computer-Aided Design* **77**, 1–17.